A&A 558, A87 (2013)
DOI: 10.1051/0004-6361/201321275

Astronomy & Astrophysics

High resolution mapping of CO(1–0) in NGC 6240⋆,⋆⋆

C. Feruglio[1], F. Fiore[2], E. Piconcelli[2], C. Cicone[3], R. Maiolino[3], R. Davies[4], and E. Sturm[4]

[1] IRAM – Institut de RadioAstronomie Millimétrique, 300 rue de la Piscine, Domaine Universitaire, 38406 Saint-Martin d'Hères, France
e-mail: feruglio@iram.fr
[2] INAF – Osservatorio astronomico di Roma, via Frascati 33, 00040 Monteporzio Catone, Italy
[3] Cavendish Laboratory, University of Cambridge, 19 J. J. Thomson Ave., Cambridge CB3 0HE, UK
[4] Max-Planck-Institut fur Extraterrestrische Physik (MPE), Giessenbachstr. 1, 85748 Garching, Germany

Received 11 February 2013 / Accepted 1 July 2013

ABSTRACT

We present long baseline CO(1–0) mapping of the luminous infrared galaxy NGC 6240 obtained with the IRAM - Plateau de Bure Interferometer. This source is a well known early-stage merging system hosting two active galactic nuclei (AGN). We find a broad CO(1−0) line profile with maximum velocity 800 km s^{-1} and a total line width of 1400 km s^{-1} that displays several kinematic components, revealing the complexity of the gas dynamics in this system. We detect a blueshifted CO emission with velocity between −200 and −500 km s^{-1}, which peaks around the southern AGN at the same position where the H_2 outflow is located. We interpret this blueshifted component as an outflow with a mass loss rate of ∼500 $M_\odot$ yr^{-1}, originating from the southern nucleus. The spatial and spectral match strongly suggests that the CO outflow is connected to the H_2 superwind located around the southern AGN and to the large scale CO outflow with similar velocities extended on scales of ∼10 kpc. The large mass loading factor ($\dot{M}/SFR \sim 10$) of the molecular gas suggests that the outflow is likely driven by both SNa winds and the radiation of the southern AGN. We discovered a nuclear, redshifted CO emission peaking in the midpoint of the two nuclei, as is the case for the CO emission at the systemic velocity. The large velocity dispersion, which reaches its maximum (∼500 km s^{-1}) in the midpoint between the two nuclei, suggests that the gas might be highly turbulent in this region, although the presence of an unresolved rotation component cannot be ruled out.

Key words. galaxies: active – galaxies: evolution – galaxies: ISM – galaxies: interactions – galaxies: individual: NGC 6240

1. Introduction

Galaxy encounters and feedbacks from active galactic nuclei (AGN) and SNe represent key processes in hierarchical galaxy formation and evolution. Mergers modify the galaxy morphology, destabilize cold gas, and trigger both star formation and nuclear accretion onto massive black holes (MBH), therefore inducing AGN activity (Sanders et al. 1988; Barnes & Hernquist 1996; Cavaliere & Vittorini 2000; Di Matteo et al. 2005). Simulations of major mergers of disk galaxies with a low gas-to-star content ratio are able to broadly reproduce the properties of local early type galaxies (Barnes & Hernquist 1996; Mihos & Hernquist 1996; Bournaud et al. 2004; Hoffman et al. 2010). Mergers of gas-rich disk galaxies may easily form massive clumps due to internal instabilities and lead to the formation of irregular spheroids with high local velocity dispersion (typically 150−200 km s^{-1}, Bournaud et al. 2011). AGN and starburst feedbacks are also expected to affect the evolution of galaxies by heating the interstellar medium (ISM) through winds, outflows and shocks, thus inhibiting further accretion onto MBH and quenching star formation on nuclear and possibly larger scales in the galactic disk of the host (Silk & Rees 1998; King 2010 and references therein). Radiative feedback from a luminous AGN and/or mechanical feedback from AGN jets could explain the low gas content of local massive galaxies and the galaxy bimodal color distribution (Kauffmann et al. 2003; Croton et al. 2006; Menci et al. 2006; Faucher-Giguere & Quataert 2012). Evidence is mounting for AGN feedback as a mechanism contributing to the transformation of AGN host galaxies. Massive, spatially extended outflows have been recently discovered in several local ultra-luminous and luminous infrared galaxies (U/LIRG) and quasars (QSO, Feruglio et al. 2010; Fischer et al. 2010; Alatalo et al. 2011; Sturm et al. 2011; Aalto et al. 2012; Cicone et al. 2012; Maiolino et al. 2012; Feruglio et al. 2013: F13 hereafter).

NGC 6240 offers the opportunity to study the intermediate phase of a merger event between the first encounter and the final coalescence (see e.g. Sanders & Mirabel 1996; Mihos & Hernquist 1996). NGC 6240 is a massive object, resulting from the merger of two gas rich spirals. The remnants of the bulges of the progenitor galaxies, separated by ∼2″ along a position angle of 40 degrees, are located in the central region of the system (Engel et al. 2010). Each of them hosts an AGN with black hole masses exceeding 10^8 $M_\odot$ (Engel et al. 2010). Both the AGNs are highly obscured by a hydrogen column of $N_H > 10^{24}$ cm^{-2} (Compton-thick AGN, Komossa et al. 2003). The southern AGN has an intrinsic luminosity of $L(2-10\ \mathrm{keV}) > 10^{44}$ erg s^{-1} (Vignati et al. 1999). Observations of CO(1–0), CO(2–1) and CO(3–2) emission lines have shown that most of the molecular gas, unlike the stellar component, is located in the region between the two nuclei (Tacconi et al. 1999; Iono et al. 2007; Engel et al. 2010, F13). The origin of this central concentration is still debated and is not reproduced by current simulations of major

⋆ Based on observations carried out with the IRAM Plateau de Bure Interferometer. IRAM is supported by INSU/CNRS (France), MPG (Germany) and IGN (Spain).

⋆⋆ Reduced datacube as a FITS file is only available at the CDS via anonymous ftp to cdsarc.u-strasbg.fr (130.79.128.5) or via http://cdsarc.u-strasbg.fr/viz-bin/qcat?J/A+A/558/A87

mergers of gas-rich galaxies. Tacconi et al. (1999) found evidence of coherent rotation in the central concentration and ascribed it to a rotating molecular disk, although with unusually large velocity dispersion. Recent high resolution observations of CO(3–2) with the SMA resolved the central concentration into two asymmetric peaks, separated by less than 1 arcsec, that are interpreted as the two gas reservoirs of the merging galaxies stripped off from the stellar systems, and tidally falling into the dynamical center of the system (U et al. 2011).

NGC 6240 displays the brightest line emission from hot molecular hydrogen (H_2) among all LIRGs. The H_2 emission peaks close to the southern AGN, unlike the CO emission, which reaches its maximum in the midpoint between the two AGNs (Tecza et al. 2000; Ohyama et al. 2003; Engel et al. 2010). The huge luminosity of H_2 (2×10^9 $L_\odot$, Egami et al. 1999; Tecza et al. 2000) is due to two main processes: the expanding motion of a shell-like structure around the southern nucleus (super-wind) and cloud-crushing at the interface of the two merging nuclei, where the superwind interacts with the central concentration of molecular gas (Ohyama et al. 2000, 2003).

The large scale, butterfly-shaped emission-line nebula seen in *Hubble* Space Telescope Hα images and in the X-rays is interpreted as evidence of a superwind, shock-heating ambient ISM (Gerssen et al. 2004; Wang et al. 2013 and references therein). The Hα and X-ray emitting filaments and bubbles appear to trace a bipolar outflow, aligned east-westward. It extends up to 15−20 arcsec (7−10 kpc) from the nuclear region, approximately perpendicular to the line connecting the two nuclei. The superwind is likely powered by both the nuclear star-formation and the southern AGN. F13 recently reports the detection of large scale structures of CO extended on 10 kpc scales, which possibly trace an outflow. Recently, Sturm et al. (in prep.) detected a P-Cygni profile absorption line of OH with *Herschel*-PACS with velocities similar to those found in CO(1−0) that unambiguously traces a molecular outflow, although the outflow was not spatially resolved due to the *Herschel* point-spread function.

In this work we present high spatial resolution observations of CO(1−0) in NGC 6240 obtained with the IRAM Plateau de Bure Interferometer (PdBI) using the long baseline array (A array configuration). F13 presents an analysis of the extended CO emission of NGC 6240 on scales of ∼10 kpc around the nuclei, whereas this paper focuses on the nuclear region, close around the two AGN and the two merging bulges. All positions, fluxes, and sizes are derived from fitting the visibilities in the uv plane, unless differently stated. A ΛCDM cosmology (H_0 = 71 km s^{-1} Mpc^{-1}; Ω_M =0.3; Ω_Λ = 0.7) is adopted.

2. PdBI observations and data analysis

We used the PdBI to observe the CO(1−0) transition, redshifted to 112.516 GHz assuming a systemic velocity of 7339 km s^{-1} (Iono et al. 2007) which corresponds to a redshift of z = 0.02448. The observations were carried out in January 2012 with five antennas in the extended (A) array configuration.

Data were calibrated using GILDAS. The system temperatures during the observations were in the range between 150 and 300 K. The on-source time, after merging all the data and after flagging the bad visibilities, is 10 hours. The absolute flux calibration relies on the strong quasars 3C 273 and 3C 279, and its accuracy is expected to be of the order 10%. The synthesized beam obtained by using natural weighting is 1.27″×0.85″, with PA = 41 deg. The achieved noise level is 2 mJy/beam over 10 MHz (i.e. ∼26 km s^{-1}). Robust weighting yields a slightly higher spatial resolution (synthesized beam of 1.20″ × 0.85″) but degrades the sensitivity to 2.5 mJy/beam in 10 MHz channels. The sensitivity of the data from the D configuration alone is degraded by a factor ∼1.5, compared to the merged A+D configuration data. The gain in spatial resolution is, however, a factor 1.8 on average. This work makes use of the A configuration data only, since a) we aim at reaching the maximum spatial resolution in the nuclear region of NGC 6240; and b) the CO emitting components presented in this paper are all detected with a significance >10σ (see Sect. 3), so the degraded sensitivity is not an issue.

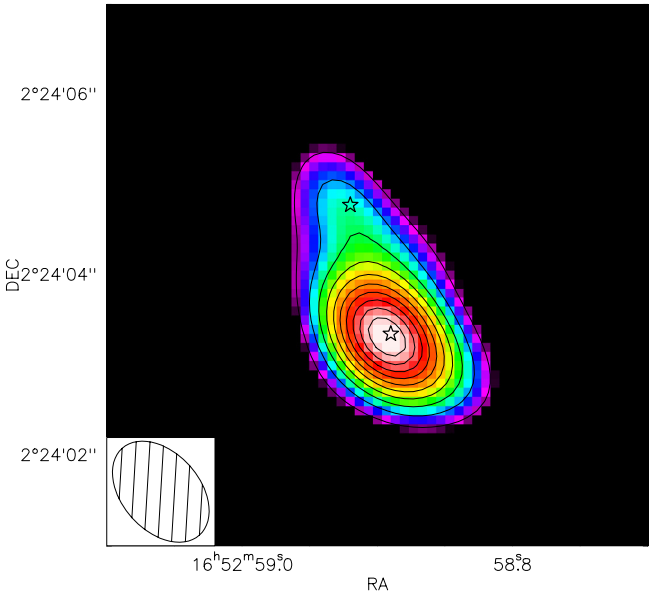

Fig. 1. 3 mm continuum map of NGC 6240 based on natural weighting. The VLBI positions of the two AGN are indicated by stars. The contours are spaced by 3σ, starting from 5σ. The oval shows the synthesized beam.

3. Results

3.1. 3 mm continua

The 3 mm continuum was estimated in a region free from emission lines (i.e., in the velocity ranges from −3500 to −2000 km s^{-1} and from 2000 to 4000 km s^{-1}). The 3 mm continuum is extended and resolved into two components, each coincident with the VLBI position of the two AGN (Hagiwara et al. 2011, Fig. 1). Most of the continuum emission is centered on the southern AGN. The strength of the 3 mm continuum, estimated by fitting two unresolved components, is 8.7 ± 0.9 mJy for the southern component and 2.9 ± 0.4 mJy for the northern one. This agrees within the expected accuracy of our measurements with the 3 mm continuum measured from the D-array configuration data (12.7 ± 1.3 mJy, F13). This means that we expect little flux loss in the nuclear region due to the enhanced spatial resolution of the observations used here. The radio spectral indexes (in the range 0.6−0.7) based on 8 GHz (Colbert et al. 1994), 1 mm (Engel et al. 2010), and 3 mm measurements (from this work) support the synchrotron origin of the continua. The continuum emission was subtracted from the total visibilities to obtain the line emission spectra.

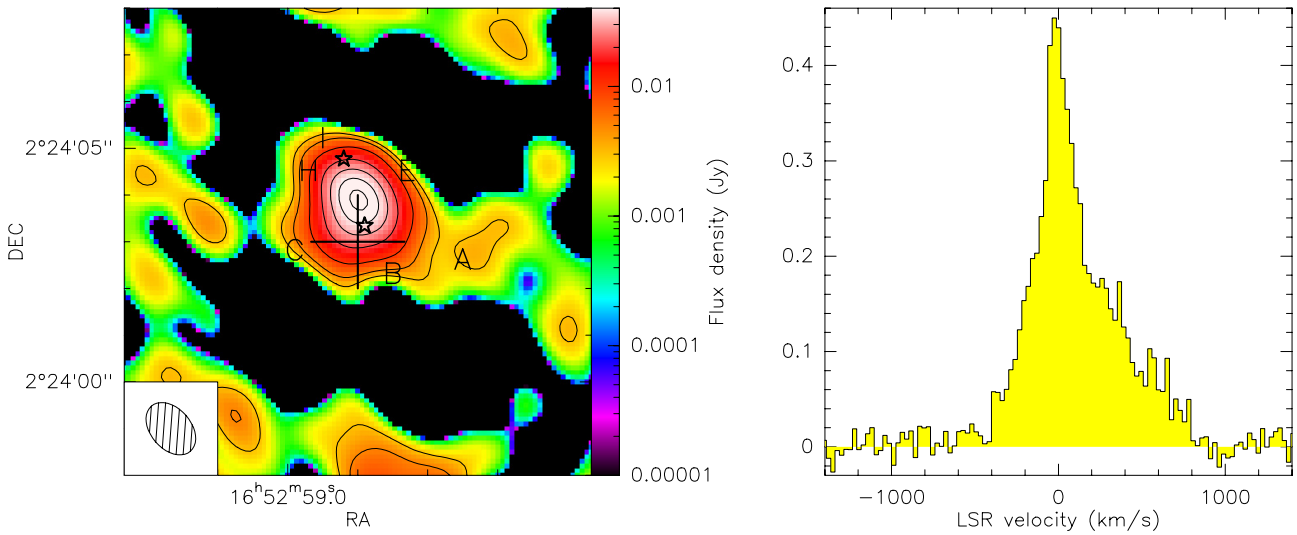

Fig. 2. *Left panel*: integrated CO(1−0) map of NGC 6240 (based on natural weighting, and in logarithmic scale in Jy). Stars indicate the positions of the two AGN. The large cross indicate the phase tracking center. The contours are 3σ, 5σ, 10σ, 20σ, 30σ, 40σ and 50σ. Labels indicate the positions where we extracted the spectra shown in Fig. 2. *Right panel*: continuum-subtracted CO line spectrum, integrated in a circular region of radius 3″ centered on the peak of CO emission. The spectral channels are 26 km s^{-1} wide.

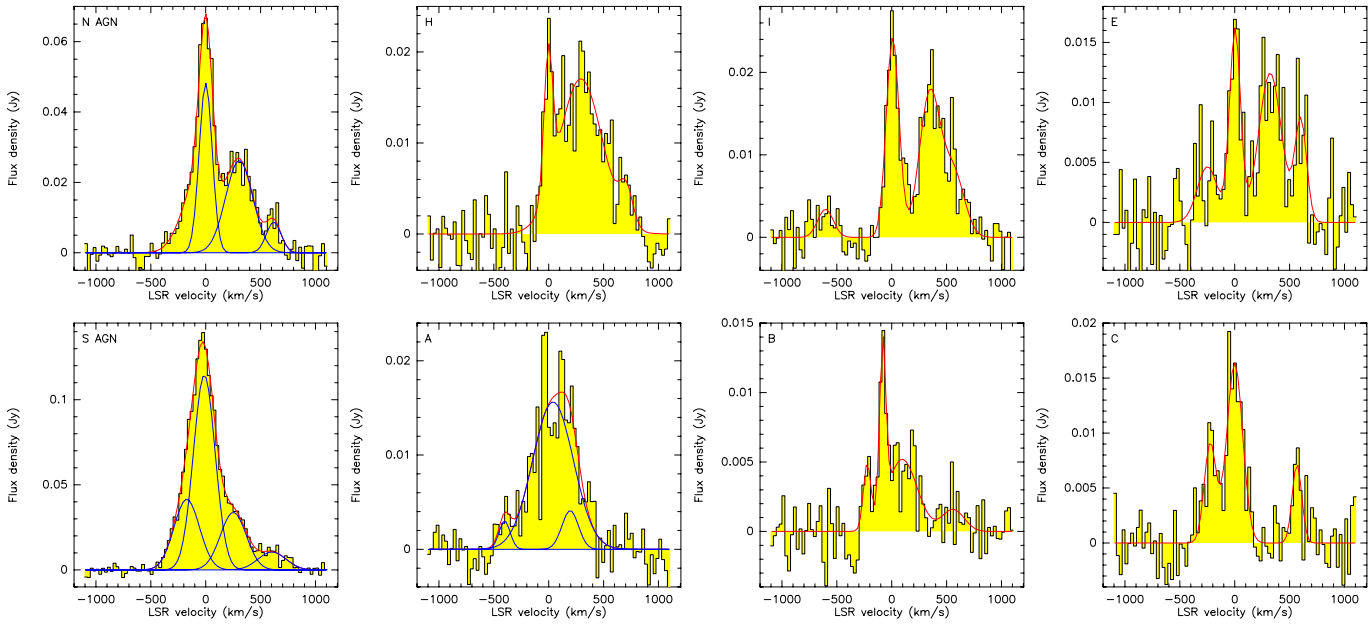

Fig. 3. Spectra at the positions marked in Fig. 1. N AGN, S AGN, A, B, C, and E are the same positions as in Tacconi et al. (1999) maps. Gaussian fitting of the profile is shown in red (total fit). Blue lines show the single Gaussian components used in the fit for the panels where the total fit is not self-explanatory.

3.2. CO(1–0) emission line

The left panel of Fig. 2 shows the continuum-subtracted, integrated map of CO(1–0). The CO(1–0) spectrum, integrated over a circular area of radius 3″ and centered on the emission peak, is shown in the right panel. The positions of the two AGN nuclei from VLBI observations (Hagiwara et al. 2011) are indicated by stars. The peak of the CO emission is centered between the two AGN, and closer to the southern AGN (S AGN). Extended fainter structures with similar morphology to those seen in the CO(2−1) maps (Tacconi et al. 1999) are visible on scales of 5″ along a position angle of 30 degrees. The CO emission line shows a complex profile, extending from −500 to 800 km s^{-1} with respect to the systemic velocity (F13). By fitting the visibilities with three elliptical Gaussian components, we find an integrated strength of the total CO(1−0) emission of 321 ± 19 Jy km s^{-1} over a total line width (FWZI) of 1400 km s^{-1}, in agreement with previous interferometric measurements (Bryant & Scoville 1996, F13).

The spectra extracted from the regions labeled as A, B, C, E, H, and I and as stars are shown in Fig. 3. These include the positions shown in Tacconi et al. (1999). The spectra show similar line profiles as those of CO(2–1) but extend out to larger velocities (up to 800 km s^{-1}) on the red side of the line. Several kinematic components are detected at different velocities. The spectrum at the position of the northern AGN (N AGN) shows a pronounced and well defined triple peak profile (peaking at velocities of $v \sim 0, 300, 600$ km s^{-1}, Table 1). The spectra at the

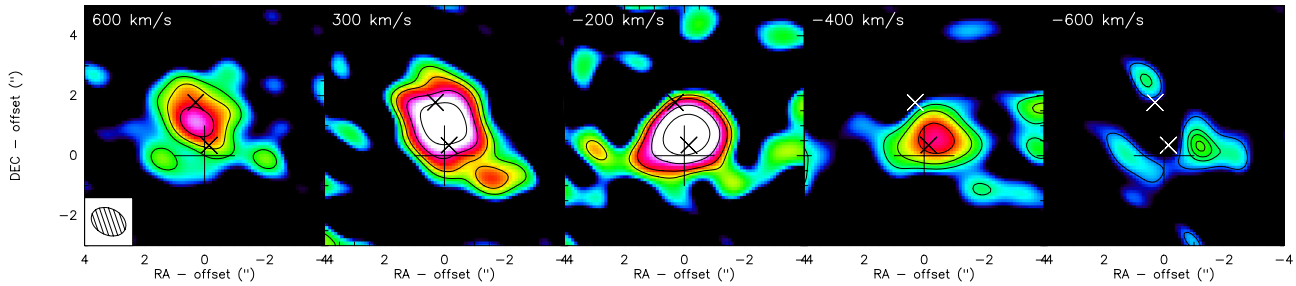

Fig. 4. Channel maps (derived using robust weighting) centered on the velocity peaks as seen in Fig. 3 and averaged over a velocity range equal to the FWHM of the corresponding Gaussian fit. Contours correspond to 3σ, 5σ, 10σ and 20σ (3σ, 5σ, 6σ, 7σ in the *rightmost panel*). The small crosses show the positions of the AGN. The large cross indicate the phase tracking center.

Table 1. Parameters of the Gaussian fit of the CO-emitting components shown in Fig. 3.

Component	I_{peak} [Jy]	v, CO(1–0) [km s^{-1}]	*FWHM* [km s^{-1}]
N AGN	$4.8 \pm 2 \times 10^{-2}$	$0. \pm 5.0$	227 ± 145
	$2.6 \pm 0.2 \times 10^{-2}$	305 ± 49	470 ± 179
	$8.7 \pm 3\ 10^{-3}$	619 ± 40	260 ± 106
E	$4.6 \pm 2 \times 10^{-3}$	-248 ± 50	355 ± 167
	$1.6 \pm 0.2 \times 10^{-2}$	2.8 ± 9.5	193 ± 57
	$1.2 \pm 0.2 \times 10^{-2}$	322 ± 18	400 ± 105
	$8.4 \pm 3 \times 10^{-3}$	602 ± 35	204 ± 79
H	$1.5 \pm 0.3 \times 10^{-2}$	-4.0 ± 7.0	152 ± 50
	$1.7 \pm 0.1 \times 10^{-2}$	292 ± 21	755 ± 171
	$4.0 \pm 3 \times 10^{-3}$	705 ± 67	234 ± 125
I	$2.4 \pm 0.2 \times 10^{-2}$	8.6 ± 4.6	226 ± 41
	$1.6 \pm 1 \times 10^{-2}$	338 ± 28	347 ± 74
	$8.3 \pm 3 \times 10^{-3}$	540 ± 136	441 ± 274
	$3.4 \pm 2 \times 10^{-3}$	-603 ± 65	272 ± 297
S AGN	$4.2 \pm 7 \times 10^{-2}$	-173 ± 408	444 ± 393
	0.1 ± 0.1	-13 ± 59	379 ± 146
	$3.4 \pm 0.5 \times 10^{-2}$	251 ± 69	450 ± 224
	$1.0 \pm 0.3 \times 10^{-2}$	604 ± 112	488 ± 271
A	$3.0 \pm 3 \times 10^{-2}$	-402 ± 74	194 ± 128
	$1.6 \pm 0.3 \times 10^{-2}$	39 ± 42	711 ± 164
	$4.1 \pm 5 \times 10^{-3}$	195 ± 85	289 ± 172
B	$4.6 \pm 2 \times 10^{-3}$	-224 ± 23	129 ± 61
	$1.2 \pm 0.2 \times 10^{-2}$	-82 ± 4	108 ± 43
	$5.2 \pm 1 \times 10^{-3}$	96 ± 54	521 ± 220
	$1.6 \pm 1 \times 10^{-3}$	559 ± 103	384 ± 224
C	$9.1 \pm 2 \times 10^{-3}$	-224 ± 19	207 ± 77
	$1.6 \pm 0.1 \times 10^{-2}$	-4 ± 8	278 ± 61
	$7.2 \pm 2 \times 10^{-3}$	567 ± 28	167 ± 56

positions E, H and I, close to the N AGN, also show at least three spectral components, peaking at similar velocities to N AGN. The spectrum at the position of the southern AGN (S AGN) shows a profile similar to N AGN but with a larger intensity ratio between the systemic and the $v = 300$ km s^{-1} components. Conversely, the spectrum at the position A lacks the $v \sim 600$ km s^{-1} component, which is present in the spectra of B and C. Blueshifted components at $v \sim -200$ km s^{-1} and $v \sim -400$ km s^{-1} appear at the positions of S AGN, A, B, and C.

Figure 4 shows channel maps integrated over a bandwidth corresponding to the FWHM and centered on the velocities that correspond to the main peaks fitted in Table 1. Both the systemic and the redshifted gas peak in the midpoint between the two nuclei, which is similar to that found by Tacconi et al. (1999), Iono et al. (2007), and Engel et al. (2010) for CO(2−1) and CO(3−2) emissions. The $v \sim 300$ km s^{-1} and $v \sim 600$ km s^{-1} redshifted

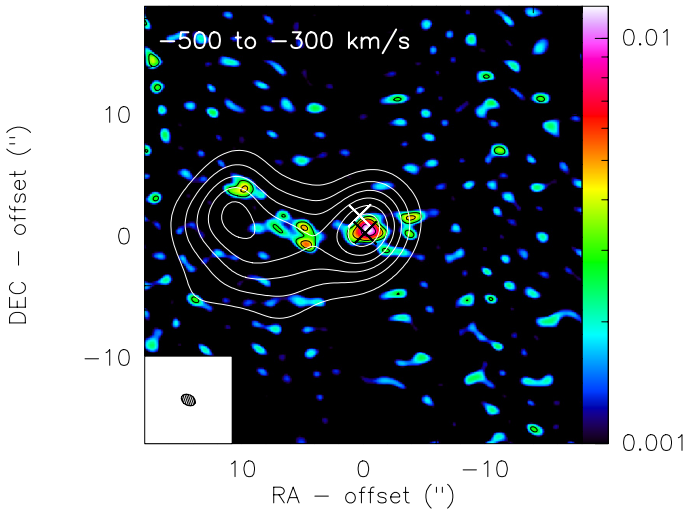

Fig. 5. Map of CO emission integrated over –500 to –300 km s^{-1} and with size 36″ × 36″. Black contours 3σ, 5σ, 10σ and 20σ. The crosses show the positions of the two AGN. White contours (5σ to 30σ, by 5σ) show the detection of the large-scale structures in the D configuration data, integrated in the range from –400 to –340 km s^{-1} (from F13).

gas is elongated along a position angle of 40 degrees, with a size of ∼5 arcsec (∼2 kpc). The integrated flux density of the high-velocity, redshifted component is 7.6 ± 0.5 Jy km s^{-1} in the velocity range 500 to 800 km s^{-1} (corresponding to 2% of the total CO emission).

The blueshifted gas is instead found closer to the position of S AGN, peaking at (–0.3, 0.6) arcsec offset from the phase tracking center. The integrated flux density of the blueshifted component, derived by fitting two Gaussian models, one elliptical and one circular, is 17.8 ± 0.6 Jy km s^{-1} over 300 km s^{-1} (in the velocity range −200 to −500 km s^{-1}), and its projected size is $\sim 2.65 \pm 0.2$ arcsec, corresponding to 1.3 kpc, in approximately the east-westward direction, by combining the sizes of the two fitted components. Figure 5 shows the same map as Fig. 4 (panel corresponding to −400 km s^{-1}) but covering the entire field of view, in order to show the extended, blueshifted CO emitting structures as discussed in F13. These extended structures are recovered by the long baseline observations, where the brightest clumps of emission are detected with a significance $>5\sigma$ out to distances of ∼10 arcsec eastwards and northeastwards of the nuclei. The clumps are aligned in a filamentary pattern that develops in the same direction of the elongation of the compact component seen close to the S AGN. Only the more compact clumps are visible, because the diffuse emission is filtered out by the interferometer. F13 showed that the extended and compact diffuse gas components are connected. The geometrical and

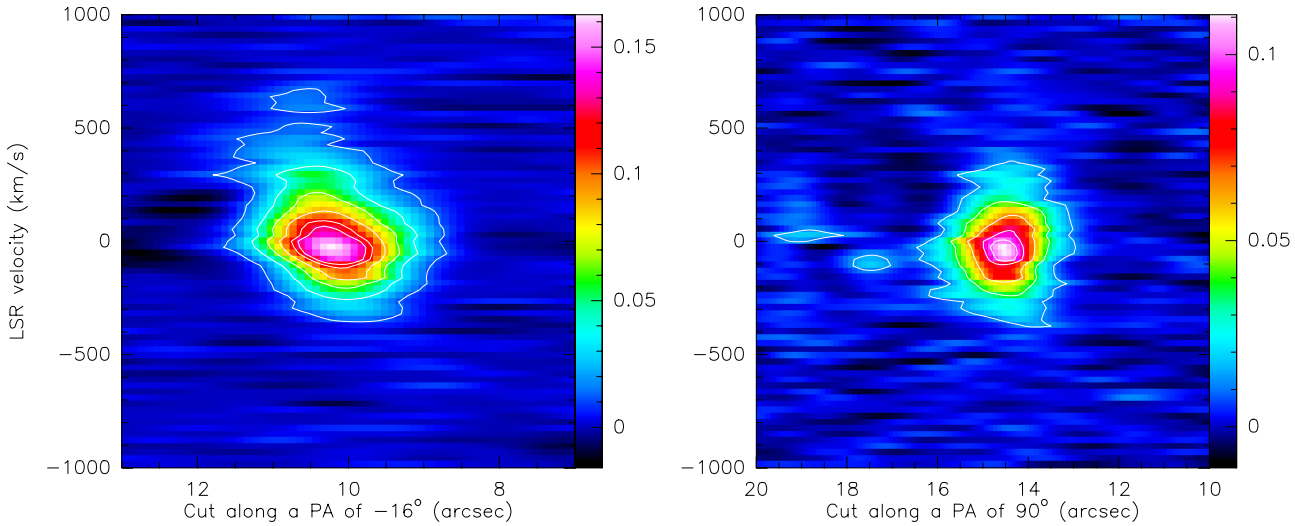

Fig. 6. Position–velocity plot cut along a PA= −16 deg, i.e. the direction of the line connecting the two nuclei, from south-west to north-east (*left panel*) and along a PA = 90 deg from north-west to south-east (*right panel*). Contours are 10σ each, starting from 5σ (σ = 2.5 mJy/10MHz).

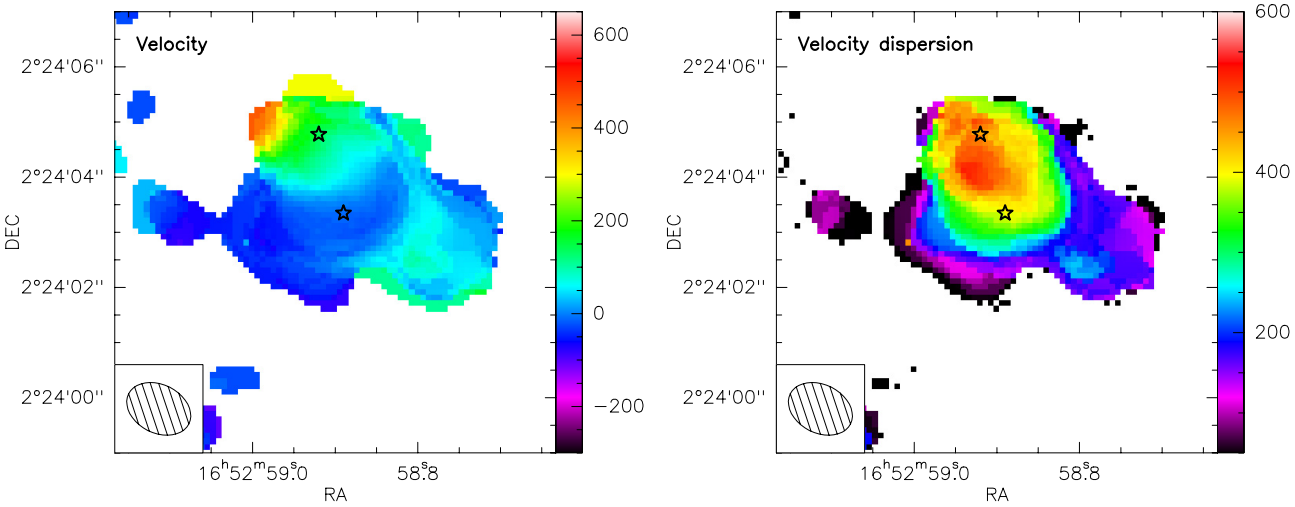

Fig. 7. *Left*: CO(1–0) velocity distribution (moment 1) map of NGC 6240. The units are in km s^{-1}. *Right*: velocity dispersion (moment 2) distribution map. Both are derived by using robust weighting to enhance the spatial resolution. Symbols are as in Fig. 1.

spectral matches suggest that the gas on large scales originates in the compact regions, although a projection effect cannot be a priori excluded. F13 interpreted the extended structures as an outflow, originating from the S AGN, although the possibility that they are a tidal streamer of gas left behind in the merging process, could not be ruled out.

Figure 6 (left panel) shows the position–velocity cut (PV diagram) along a position angle PA = 16 degrees, defined along the line connecting the two nuclei, from south-west to north-east. The gas with a velocity larger than 500 km s^{-1} is shifted to the north-eastern part of the system. Although no resolved rotation pattern is seen, the position shift of the gas in the range of ±300 km s^{-1} along the cut, which is slightly larger than the beam, suggests that there might be an unresolved rotation in the central concentration of CO. The right panel of Fig. 6 shows a cut along a PA = 90 degrees, corresponding to the direction where the blueshifted emission is elongated and intercepting the position of the S AGN. No evidence of a coherent rotation is found here. We find, however, that the gas with velocity between −200 and −400 km s^{-1} is seen everywhere along the cut on scales of ∼2.5 arcsec, as also found by fitting the visibilities. A separated component (5σ) with velocity of −200 km s^{-1} is seen at 3 arcsec eastward of the nuclei.

The offset in position between the peak of the redshifted and blueshifted emission is shown in Fig. 7 (left panel), which shows the velocity (moment 1) distribution map of CO(1–0). The velocity gradient between the two AGN is ∼150 km s^{-1}. Figure 7 (right panel) shows the line-of-sight velocity dispersion (moment 2) map. This reaches its maximum (∼500 km s^{-1}) in the central CO concentration and in the region around the N AGN.

4. Discussion

We have mapped the CO(1–0) emission line in NGC 6240 with the extended A configuration of the PdBI, reaching an average spatial resolution of ∼500 pc at the redshift of the source. The 3 mm continuum shows two components, coincident with the position of the two AGN. Our 3 mm measurements confirm the non-thermal synchrotron origin of the continua (Engel et al. 2010, and references therein).

Thanks to the large bandwidth available today at the PdBI (3.6 GHz), we have detected a broad CO(1–0), reaching larger redshifted velocities than those previously reported (Tacconi et al. 1999; Iono et al. 2007; Engel et al. 2010). The CO emission at different locations of the system shows similar line profiles to those of CO(2–1) (Tacconi et al. 1999; Engel et al. 2010), but with a larger line width and exhibits several kinematic components (blue- and redshifted, compared to the systemic one, Table 1). We confirm that the molecular gas is concentrated between the two AGN in what is known as the central concentration.

The total integrated luminosity of the CO line is $L'(\mathrm{CO}) = 8.6 \times 10^9$ K km s^{-1} pc^2, including the central concentration and the extended structure. Assuming the conversion factor typically used for ULIRGs, $\alpha = 0.8$ (Solomon et al. 1997), we derive a total mass of molecular gas of $M(\mathrm{H_2}) = 6.8 \pm 0.7 \times 10^9$ $M_\odot$. This agrees with the estimate of $6.8 \pm 1.7 \times 10^9$ $M_\odot$, based on CO(3–2), reported by Iono et al. (2007). The luminosity of CO in the central 1 kpc region is $L'(\mathrm{CO}) = 5 \times 10^9$ K km s^{-1} pc^2 over a line width of 1400 km s^{-1}. This converts into a molecular gas mass of $M(\mathrm{H_2}) = 4 \times 10^9$ $M_\odot$, consistent with the mass derived from CO(2−1) (Engel et al. 2010).

We report the discovery of a new nuclear component of CO(1–0) at redshifted velocities larger than 500 km s^{-1} and up to 800 km s^{-1} with respect to the systemic CO-derived velocity. The luminosity of this component is $L'(\mathrm{CO}) = 2 \times 10^8$ K km s^{-1} pc^2. The inferred mass of molecular gas is $M(\mathrm{H_2}) = 1.6 \times 10^8$ $M_\odot$, assuming $\alpha = 0.8$. The possible existence of this component was suggested by Tacconi et al. (1999) and Engel et al. (2010) based on CO(2−1), although no direct evidence of such emission has been reported due to the narrow bandwidth. Interestingly, and similarly to what found for CO(2−1), the redshifted and the blueshifted emission peaks are offset. The latter is concentrated closer to the S AGN compared to the redshifted component, which peaks at the same position of the central concentration (Fig. 4). This observation was interpreted as evidence of a rotating, turbulent molecular disk (Tacconi et al. 1999). In contrast, Engel et al. (2010) argued that it was more likely to be a bridge of gas, which would be prominent for a merger geometry that is not too far from co-planar and prograde. They also noted, however, that the CO-to-H_2 conversion factor would have to be high for the gas mass to be consistent with models, as it is the case of non-virialised clouds. Our data can hardly be reconciled with one turbulent, rotating disk. The large velocity observed (800 km s^{-1}), and the lack of a corresponding blueshifted component rule out the rotating disk hypothesis. U et al. (2011) suggest that the large velocity gradients seen in the nuclear region are two rotating disks (the original gas reservoirs of the merging bulges) orbiting the dynamical center of the system. The spatial resolution of our data does not allow us to confirm or discard this hypothesis. Current hydrodynamical simulations of mergers of gas rich galaxies (Bournaud et al. 2011) predict the formation of clumps, producing an emission line profile with multiple components. The velocity dispersions due to turbulence can reach 150–200 km s^{-1}, and even 500 km s^{-1} in these systems, when projected along some lines of sight. These simulations describe mergers of high redshift galaxies, like SMGs, for which the molecular gas is expected to be more turbulent than in local galaxies. NGC 6240 is a merger of two massive, gas-rich galaxies, a rare case in the local universe, but common among high redshift galaxies. The origin of the huge concentration of gas in the midpoint of the two nuclei is, however, still debated and not explained by current models of merging systems.

The blueshifted emission with a velocity of −200 km s^{-1} peaks at a position of 0.4 arcsec northward of the S AGN, the same position of the H_2 peak (Ohyama et al. 2000, 2003). The blueshifted CO with $v = -400$ km s^{-1} is also found close to the S AGN, matching the H_2 outflow component with similar velocity (Ohyama et al. 2000, 2003; Engel et al. 2010). The H_2 blueshifted components with velocities −200 and −500 km s^{-1} are interpreted as arising from super-wind activity in the southern nucleus. These spatial and kinematic matches strongly suggest that the CO blueshifted emission is associated with the H_2 emitting expanding shell, originating from the southern nucleus. The blueshifted component has $L'(\mathrm{CO}) = 4.7 \pm 0.2 \times 10^8$ K km s^{-1} pc^2, corresponding to a mass of molecular gas of $M(\mathrm{H_2}) = 2.4 \pm 0.2 \times 10^8$ $M_\odot$, assuming $\alpha = 0.5$ (Weiss et al. 2001; Feruglio et al. 2010). Assuming that the outflow is symmetric along the major axis (bi-conical geometry), that $R_{\rm of} = 0.6 \pm 0.1$ kpc, and that the terminal de-projected velocity is equal to the maximum blueshifted velocity $v_{\rm of} = -400$ km s^{-1}, we derive a lower limit mass loss rate using the relation of Feruglio et al. (2010) and Maiolino et al. (2012):

$$\dot{M} = \frac{3 \times v_{\rm of} \times M(\mathrm{H_2})}{R_{\rm of}} \simeq 500\ M_\odot\ \mathrm{yr}^{-1}, \quad (1)$$

assuming that the (bi)cone is uniformly filled with gas (or with gas clouds) and that there is no mass loss through the lateral sides of the cone. The kinetic power entrained in the outflow is $P_{\rm k,OF} = 0.5 \times \dot{M} \times v_{\rm of} \simeq 3 \times 10^{43}$ erg s^{-1}. The nuclear star-formation rate measured from FIR SED fitting is $60 \pm 30\ M_\odot$ yr^{-1} (Yun & Carilli 2002). The derived mass loading factor of the molecular gas, $\dot{M}$/SFR in the range 8−17, suggests that the AGN contributes to the molecular outflow, in addition to the SNa winds. According to the relation of Veilleux et al. (2005), SNe can power winds with a maximum kinetic power of $P_{\rm k,SF} = 4{-}7 \times 10^{42}$ erg s^{-1} at the rate found for NGC 6240. By fitting the nuclear component from the short baseline data only in the same spectral range, and using the same assumptions, we get a mass of molecular gas $M(\mathrm{H_2}) = 1.8 \pm 0.4 \times 10^8$ $M_\odot$ and a mass loss rate in the range 300 to 450 $M_\odot$ yr^{-1}. Accounting for the 10% uncertainty in the flux calibration, the two estimates are consistent. Conversely, we find a discrepancy when comparing the compact outflow with that extended eastwards on 10 kpc scale (F13), which has a $\dot{M} \sim 100$ $M_\odot$ yr^{-1}. We discuss possible reasons for this discrepancy, in addition to the mis-knowledge of the conversion factor α, which might be different in the compact region compared to the extended one. Contrary to what is assumed in our simple scenario, the eastern extended cone does not appear to be uniformly filled with gas. When seen with high spatial resolution it shows clumps of emission of different sizes and brightnesses. Moreover, the mass loss rate is not conserved with increasing radius if a significant amount of gas is lost through the lateral sides of the cone.

Finally, the similar spatial resolution of our maps and of those of CO(2–1) (Tacconi et al. 1999) allow us to compare the line strengths in different locations of the system, such as the central kpc and the extended region on scales of 3 arcsec around the nuclei. Figure 1 shows that the CO(1–0) emission exhibits a very similar extension and similar structures to that of CO(2−1). We measured the total emission in two apertures centered on the emission peak with radii of 1 and 1.5 arsec each. In the central 1 kpc region around the central concentration, we find $L'(\mathrm{CO}) = 3.4 \times 10^9$ K km s^{-1} pc^2 in the velocity range of −500 to 500 km s^{-1}. Tacconi et al. (1999) measured a flux of CO(2–1) equal to 528 Jy km s^{-1} for the central 1 kpc region and a total

flux density of 1220 Jy km s^{-1} in a 1.5 kpc region in the same velocity range. The ratio, $L\,CO_{(2-1)}/L\,CO_{(1-0)} = 1.0$, for the central concentration indicates that the gas there is moderately optically thick. The integrated flux density in the extended region around the two nuclei is $L'(CO) = 1.2 \times 10^9$ K km s^{-1} pc^2, which gives $L\,CO_{(2-1)}/L\,CO_{(1-0)} \sim 3.8$, suggesting that the gas here is instead optically thin.

5. Summary

We present high spatial resolution CO(1–0) imaging of the luminous infrared galaxy NGC 6240 obtained with the PdBI. We provide our main findings below:

1. We find a broad CO(1–0) line profile with a maximum velocity of 800 km s^{-1} and *FWZI* = 1400 km s^{-1} with several kinematic components, witnessing the complexity of the gas dynamics in this source. The CO emission peaks in the midpoint between the two nuclei, as found in previous studies (Engel et al. 2010 and references therein). This component is not predicted by recent hydrodynamical simulations of mergers between gas rich galaxies (Bournaud et al. 2011).
2. The blueshifted CO emission with −200 and −500 km s^{-1} peaks close to the S AGN at the same position where a H_2 outflow is found. Based on this and on the evidence that an outflow is also seen with similar velocities in absorption with *Herschel*-PACS (Sturm et al. in prep.), we regard this result as a clear indication of a massive molecular outflow, expanding from the southern nucleus. Its mass loss rate is at least 500 $M_\odot$ yr^{-1}, and the mass loading factor of the molecular gas, $\dot{M}$/SFR, is of the order of 10. The CO outflow is likely connected to the H_2 superwind around the southern nucleus (Ohyama et ao 2000, 2003) and to the large scale CO outflow, found on scales of 10 kpc. The latter shows similar velocities and a filamentary structure that appears connected to the S AGN (F13). The molecular compact outflow is likely driven by both AGN and SNe.
3. The redshifted CO emission, which shows a maximum velocity of 800 km s^{-1}, peaks at the midpoint of the two nuclei, as is the case for the systemic CO. The most redshifted gas is shifted towards the northern part of the system (close to N AGN). The gas is probably turbulent in the nuclear region, as supported by the large velocity dispersion, which reaches its maximum (∼500 km s^{-1}) in the central CO concentration. We suggest that this component of the molecular gas is flowing towards or, perhaps, orbiting around the center of mass of the system, where the two gas reservoirs will eventually merge. Limited by the spatial resolution of our data we cannot, however, conclude whether rotation in the center of the system occurs or not.

Interferometric observations with higher spatial resolution with ALMA will certainly add crucial constraints on the gas dynamics in NGC 6240.

Acknowledgements. We thank Dennis Downes for useful discussions. F.F. acknowledges support from PRIN-INAF 2011.

References

Aalto, S., Garcia-Burillo, S., Muller, S., et al. 2012, A&A, 537, A44
Alatalo, K. A., Davis, T. A., Young, L. M., et al. 2011, ApJ, 735, 88
Barnes, J. E., & Hernquist, L. 1996, ApJ, 471, 115
Bournaud, F., Combes, F., & Jog, C. J. 2004, A&A, 418, L27
Bournaud, F., Chapon, D., Teyssier, R., et al. 2011, ApJ, 730, 4
Bryant, P. M., & Scoville, N. Z. 1996, ApJ, 457, 678
Cavaliere, A., & Vittorini, V. 2000, ApJ, 543, 599
Cicone, C., Feruglio, C., Maiolino, R., et al. 2012, A&A, 543, A99
Colbert, E. J. M., Wilson, A. S., & Bland-Hawthorn, J. 1994, ApJ, 436, 89
Croton, D. J., Springel, V., White, S. D. M., et al. 2006, MNRAS, 367, 864
Di Matteo, T., Springel, V., & Hernquist, L. 2005, Nature, 433, 604
Egami, E. 1999, Ap&SS, 266, 105
Engel, H., Davies, R. I., Genzel, R., et al. 2010, A&A, 524, A56
Faucher-Figuere, C.-A., & Quataert, E. 2012, MNRAS, 425, 605
Feruglio, C., Maiolino, R., Piconcelli, E., et al. 2010, A&A, 518, A155
Feruglio, C., Fiore, F., Maiolino, R., et al. 2013, A&A, 549, A51
Fischer, J., Sturm, E., Gonzales-Alfonso, E., Gracia-Carpio, J., Hailey-Dunsheath, S., et al. 2010, A&A, 518, L41
Gerssen, J., van der Marel, R. P., Axon, D., et al. 2004, AJ, 127, 75
Hagiwara, Y., Baan, W. A., & Klockner, H. 2011, AJ, 142, 17
Hoffman, L., Cox, T. J., Dutta, S., & Hernquist, L. 2010, ApJ, 723, 818
Iono, D., Wilson, C. D., Takakuwa, S., et al. 2007, ApJ, 659, 283
Kauffmann, G., Heckman, T. M., Tremonti, C., et al. 2003, MNRAS, 346, 1055
King, A. R. 2010, MNRAS, 402, 1516
Komossa, S., Burwitz, V., Hasinger, G., et al. 2003, ApJ 582, 15
Maiolino, R., Gallerani, S., Neri, R., et al. 2012, MNRAS, 425, 66
Menci, N., Fontana, A., Giallongo, E., et al. 2006, ApJ, 647, 753
Menci, N., Fiore, F., Puccetti, S., & Cavaliere, A. 2008, ApJ, 686, 219
Mihos, J. C., & Hernquist, L. 1996, ApJ, 464, 641
Ohyama, Y., Yoshida, M., Takata, T., et al. 2000, PASJ, 52, 563
Ohyama, Y., Yoshida, M., & Takata, T. 2003, AJ, 126, 229
Riffel, R. A., Storchi-Bergmann, T., Winge, C., et al. 2008, MNRAS, 385, 1129
Sanders, D. B., & Mirabel, I.F. 1996 ARA&A, 34, 749
Sanders, D. B., Soifer, B. T., Elias, J. H., et al. 1988, ApJ, 325, 74
Scoville, N. Z., Frayer, D. T., Schinnerer, E., & Christopher, M. 2003, ApJ, 585, L105
Silk, J., & Rees, M. J. 1998, A&A, 331, L1
Sturm, E., Gonzalez-Alfonso, E., Veilleux, S., et al. 2011, A&A, 518, A36
Solomon, P. M., Downes, D., & Radford, S. J. E. 1997, ApJ, 478, 144
Tacconi, L., Genzel, R., Tezca, M., & Gallimore, J. F. 1999, ApJ, 524, 732
Tecza, M., Genzel, R., Tacconi, L. J., et al. 2000, ApJ, 537, 178
U, V., Wang, Z., Sanders, D., et al. 2011, ASPC, 446, 97
Van der Werf, P., Genzel. R., Krabbe, A., et al. 1993, ApJ, 405, 522
Veilleux, S., Cecil, G., & Bland-Hawthorn J. 2005, ARA&A, 43, 769
Vignati, P., Molendi, S., Matt, G., et al. 1999, A&A, 349, 57
Yun, M. S. & Carilli, C. L. 2002, ApJ, 568, 88
Wang, J., Nardini, E., Fabbiano, G., et al. 2013, ApJ, submitted [arXiv:1303.2980]
Weiss, A., Neininger, N., Hüttemeister, S., & Klein, U. 2001, A&A, 365, 571